The Structure of D-Erythro-C18 Ceramide at the Air-Water Interface

David Vaknin and Michael S. Kelley
Ames Laboratory and Department of Physics and Astronomy, Iowa State University, Ames, Iowa 50011 USA

ABSTRACT X-ray reflectivity (XR) and diffraction at grazing angles of incidence (GID) were conducted to determine the structure of synthetic D-erythro C18-ceramide films at the air-water interface at various surface pressures (π). Analysis of the GID reveals that the monomolecular film, at the crystalline phase ($\pi > 0$ mN/m), is predominantly hexagonal. In this crystalline phase, the analysis of the reflectivity yields an electron density profile that consists of three distinct homogeneous slabs, one associated with the headgroup region and the other two with the hydrocarbon chains. At large molecular areas ($\pi \approx 0$), isolated crystalline domains coexist with two-dimensional gas phase. Within the crystalline domains, we find an orthorhombic arrangement of the chains that coexists with the hexagonal symmetry. It is argued that the two-dimensional orthorhombic crystals are induced by hydrogen bonding between headgroups even at very low surface pressures. Although their structure is incommensurate with the simple hexagonal arrangement, they act as nucleation centers for the conventional hexagonal phase which dominates at high π.

INTRODUCTION

Ceramides, the N-acylated derivatives of sphingosine, belong to the diverse family of sphingolipids that are abundant in brain tissues, predominating the myelin sheath of nerve fibers (Spiegel and Merrill, 1996). Sphingolipids are also found in a variety of mammal tissues albeit in smaller quantities compared to other lipids. Recently, interest in this family of lipids was stimulated by findings that demonstrated that they play important active roles in the functions of living cells. The sphingolipids are not merely passive constituents of cell membranes but, they participate in a variety of activities in the cellular life cycle, including growth, differentiation, and even programmed death. For instance, it has been shown that sphingosine is essential to cellular proliferation regulation, whereas ceramides mediate membrane-shrinking that leads to apoptosis (Hannun, 1994; Spiegel and Merrill, 1996). In addition, it was also reported that biological functionality of ceramides strongly depends on the length of the side-chain at the primary amine of sphingosine (Hauser et al., 1994).

Ceramides can also be found in the outer layer of the skin of mammals (epidermal horny layer), reptiles, and birds (Garson et al., 1991). It was hypothesized that ceramides are essential building blocks that confer structural rigidity to membranes by virtue of their ability to form strong hydrogen bonds (Abrahamsson et al., 1976). They contain amide-carbonyl, which is a hydrogen acceptor, and several hydroxyl donor groups that can form stable hydrogen bonds between neighboring molecules. Together with cholesterol, fatty acids, and polypeptides, ceramides form durable outer membranes that withstand the harsh mechanical, chemical and thermal conditions which skin tissues may be subjected to (Gray and Yardley, 1975).

We have undertaken the present X-ray scattering study to determine the structure of a pure synthetic ceramide in a monolayer at the air-water interface and to focus on surface properties that might elucidate its functions, in particular as an important constituent of the cell boundary with the environment. Although qualitative x-ray diffraction studies from bulk and lamellar structures were reported for C16-ceramide (Shah et al., 1995) and for natural ceramide consisting of a distribution of secondary chains (Bouwstra et al., 1996), very little is known about the packing of these lipids at the monolayer form.

EXPERIMENTAL DETAILS

Materials and monolayer preparation

D-erythro-C18 ceramide (2-octadecanoylamino-1,3-dihydroxy-octadecene-4), a sphingosine with an amine-linked fatty acid, see Fig. 1, was obtained from Matreya, Inc. (Pleasant Gap, PA). Samples were weighed directly into 10 mL volumetric flasks that were subsequently filled with chloroform (HPLC grade, Fisher Scientific, Fair Lawn, NJ) and sonicated to yield uniform solutions. Langmuir monolayers were prepared on pure water (Milli-Q, Millipore Corp., Bedford, MA; resistivity, 18.2 MΩcm) in a temperature-controlled Teflon trough maintained at 18 $\pm$ 1°C in a gas-tight aluminum container. Surface pressure (π) was obtained by differential weight measurements using a filter-paper Wilhelmy plate. Compression of the monolayer at a rate of $\approx$1 Å^2 per molecule per minute was started approximately 20 min after spreading the molecules from chloroform solution. During the X-ray scattering experiments, the barrier position in the Langmuir trough was adjusted regularly to keep a constant pressure within a range of $\pm$0.5 mN/m. To reduce incoherent scattering from air, and to slow down film deterioration by oxidation due to radicals produced by the beam, the monolayer was kept under a He environment during the X-ray measurements. No noticeable differences were found in the $\pi - A$ isotherms when performed under air or He.

$\pi - A$ isotherm

Figure 1 shows surface pressure versus molecular area ($\pi - A$) isotherm for ceramide at T = 18°C. Although the surface-pressure is very low down

Received for publication 22 November 1999 and in final form 10 August 2000.

Address reprint requests to David Vaknin, Department of Physics and Astronomy, Iowa State University, Ames, IA 50011. Tel.: 515-294-6023; Fax: 515-294-0689; E-mail: vaknin@ameslab.gov.

0006-3495/00/11/2616/08 $2.00

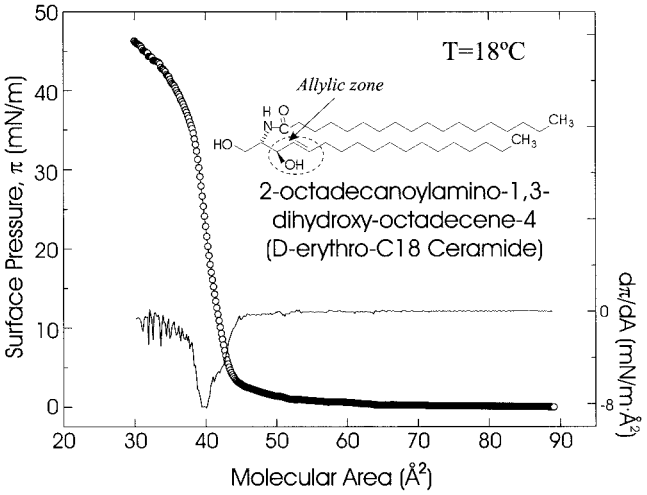

FIGURE 1 Surface pressure π and its derivative $\frac{d\pi}{dA}$ versus molecular area (A) of C18:0 ceramide on pure water. The limiting molecular area is 42 ± 1 Å^2. Fluctuations in surface pressure near 58 Å^2/molecule, indicate the condensation of crystalline domains.

to a molecular area $A \approx 45$, Å^2/molecule, pressure fluctuations below 60 Å^2 indicative of film reorganization, are observed. The surface pressure for the ceramide monolayer increases abruptly at about 45 Å^2, reaching a densely packed film at $\approx$ 40 Å^2 per molecule, just prior to collapse. Systematic studies of the $\pi - A$ isotherm (Löfgren and Pascher, 1977) led Löfgren and Pascher to postulate two-dimensional (2D) aggregation of the molecules with onset below about 58 Å^2. Furthermore, they argued that the molecules in the aggregates near zero surface pressure are closely packed with an area per lipid close to the limiting area, $A_0 = 42.0$ Å^2, implying that the chains in the aggregates are not significantly tilted from the surface normal (Löfgren and Pascher, 1977). These claims can be directly examined by XR and GID techniques presented herein.

X-ray scattering

In situ X-ray scattering experiments from spread films of ceramide at the air-water interface were carried out on a liquid-surface reflectometer at Ames Laboratory using the CuKα radiation of a rotating anode (Rigaku, UltraX 18), and on the Harvard/BNL Liquid Surface Diffractometer at the National Synchrotron Light Source (NSLS), beamline X22B, with a wavelength, $\lambda = 1.54$ Å, described elsewhere (Ocko et al., 1997; Schwartz et al., 1992). The incident beam of wave-vector $\mathbf{k}_i$ ($|k_i| = \mathbf{k}_0 = 2\pi/\lambda$) strikes the free liquid surface at a grazing angle α that can be varied by tilting the Bragg reflecting planes of a Ge(111) crystal. The diffracted beam, ($\mathbf{k}_f$), is detected at angles β with respect to the liquid surface, and transversely at 2θ with respect to the untilted incident beam, yielding a momentum transfer $\mathbf{Q}$ ($\equiv \mathbf{k}_i - \mathbf{k}_f$) with the following components:

$$Q_z = k_0(\sin\alpha + \sin\beta) = k_{z,i} + k_{z,f} \tag{1}$$

$$Q_{xy} = k_0\sqrt{\cos^2\alpha + \cos^2\beta - 2\cos\alpha\cos\beta\cos 2\theta}\,. \tag{2}$$

X-ray reflectivity (XR)

Specular XR ($\alpha = \beta$, $2\theta = 0$) experiments were conducted to determine the electron densities across the interface and to relate them to molecular arrangements in the film. The procedure for performing and analyzing XR measurements from Langmuir monolayers were described in the literature (Als-Nielsen and Kjaer, 1989) and (Ocko et al., 1997). In the Born approximation (BA), the reflectivity from a homogeneous electron density $\rho(z)$, is given by

$$R(Q_z) = R_F(Q_z)\left|\frac{1}{\rho_s}\int < \left(\frac{d\rho}{dz}\right) > e^{iQ_zZ}dz\right|^2 = R_F(Q_z)|\Phi(Q_z)|^2 \tag{3}$$

where ρ_s is the electron density of the liquid substrate, $R_F(Q_z)$ is the reflectivity of an ideally flat liquid surface, and $\Phi(Q_z)$ is the generalized structure factor of the film. A more accurate formalism to calculate the reflectivity has been used in the present study in which

$$R(Q_z) = R_0(Q_z)e^{-(Q_z\sigma)^2} \tag{4}$$

where $R_0(Q_z)$ is the reflectivity from step-like functions, calculated by the recursive dynamical method (Parratt, 1954), and σ is an effective surface roughness associated with the Debye-Waller-like term ($e^{-(Q_z\sigma)^2}$) which accounts, in the BA, for the smearing of the interfaces (mainly due to thermal capillary waves and surface imperfections) (Als-Nielsen and Kjaer, 1989). The underlying assumption in this approach is that all interfaces are smeared identically by one interfacial roughness σ (i.e., conformational roughness). By nonlinear least-squares refinement, the electron density across the interface $\rho(z)$ can be extracted, using the thicknesses of the various slabs, their electron densities, and one surface roughness as independent parameters. The number of parameters (i.e., slabs) used to fit the data is the minimum number for which the addition of extra parameters does not improve the quality of the fit.

X-ray diffraction at grazing angles of incidence (GID)

X-ray diffraction experiments at grazing angles of incidence (GID) were used to determine the lateral organization in the film. In these experiments, the angle of the incident beam with the surface (α) is fixed below the critical angle for total reflection ($\alpha_c = \sqrt{4\pi\rho_s}/k_0$), and the diffracted beam ($\mathbf{k}_f$) is detected at a finite in-plane angle 2θ. The intensity of the scattered beam along the out-of-plane angle β was measured with a linear position sensitive detector (PSD). The incident evanescent wave penetrates to a finite depth ($\sim 1/\sqrt{k_{i,z}^2 - (k_c)^2}$; $k_c \equiv k_0 \sin\alpha_c$), reducing scattering from the bulk, and increasing the sensitivity to the topmost portion of the interface ($\approx$100 Å).

RESULTS AND ANALYSIS

X-ray reflectivity

Reflectivity measurements normalized to the calculated reflectivity of ideally flat water interface R_F were conducted at various points on the $\pi - A$ isotherm, and typical scans at 101, 69, 48, and 41 Å^2 per molecule are shown in Fig. 2 *A*. These curves were obtained with the rotating anode X-ray source, where the reflectivities at the largest momentum transfer were on the order of 10^{-7} ($Q_z = 0.5$ Å^{-1}). Similar experiments at the NSLS yielded reflectivities down to 10^{-9}, reaching a higher Q_z range and better signal-to-noise ratios, as shown in Fig. 3. The two-slab model is commonly used to fit reflectivities from amphiphilic monolayers (i.e., fatty acids, lipids) where the slab contiguous to the aqueous subphase is associated with the lipid headgroup and integrated water molecules and the second slab, at the air

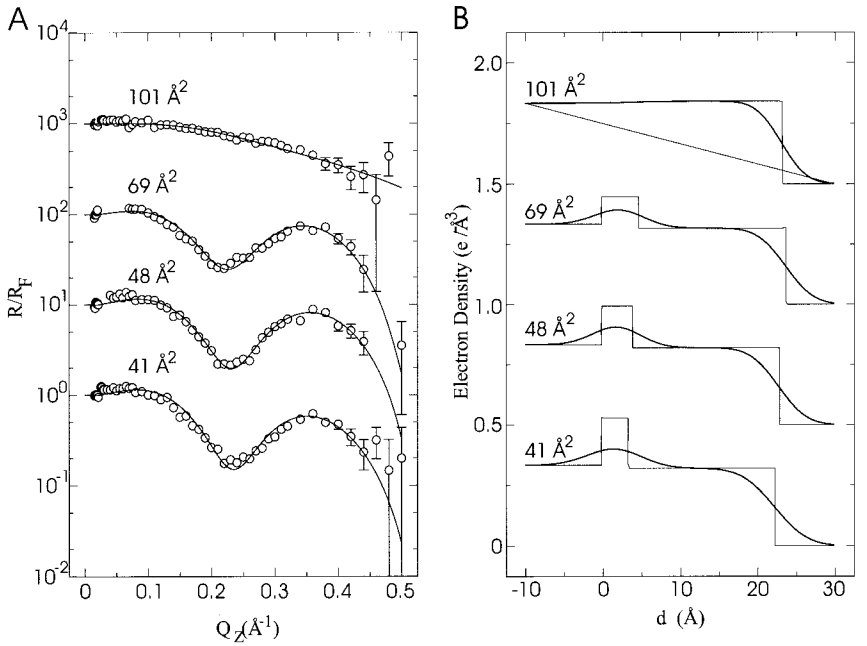

FIGURE 2 Measured reflectivity curves normalized to R_F (reflectivity from pure subphase) at various molecular areas. Experiments were performed on the rotating anode at Ames Laboratory (*A*). The solid lines are best fit two-slab model of the electron density to the data shown in (*B*). The reflectivity at $A = 69$ Å^2 per molecule was modeled by assuming incoherent scattering from densely packed domains and pure water surface, following Eq. 8.

interface, comprises the hydrocarbon chains (Als-Nielsen and Kjaer, 1989). Fig. 2 *A* shows fits to the data using the corresponding electron densities shown in Fig. 2 *B*. The analysis of the reflectivity curves taken at the synchrotron, although similar to those measured with the rotating anode, required a slight modification of the two-slab model, to comprise three slabs. The additional slab indicates that the electron density along the hydrocarbon chain region is not uniform and consists of at least two distinct densities, as shown in Fig. 3 *B*. The best fit yields an electron density of the topmost layer (Fig. 3 *C*), which is lower than that of closely packed hydrocarbon chains, but not half that of the densely packed alkyl tail region. This suggests that the interface between the low and high density hydrocarbon layer goes through the overlap section of the two chains as depicted in the molecular model in Fig. 3 *C*.

GID and rod scans from the monolayer

At all pressures, GID scans in the range $0.1 \leq Q_{xy} \leq 2.0$ Å^{-1} revealed prominent Bragg reflections in a Q_{xy} range that indicates 2D ordering of the hydrocarbon chains. Fig. 4 shows the diffraction pattern from ceramide monolayers at several molecular areas and pressures. Similar scans at smaller Q_{xy} did not reveal any low order reflections that could be assigned to the ordering of the molecular headgroups. Fig. 5 shows two in-plane diffraction scans, one taken at the horizon ($\beta = 0$) and the second taken off the horizon across the rod, at $\beta \approx 3°$, indicating that at relatively high surface-pressures a single Bragg reflection at $Q \approx 1.5$ Å^{-1} dominates the diffraction pattern. This Bragg reflection is relatively weak and broad at large molecular areas ($A \geq 58$ Å^2), and it becomes stronger and sharper and gradually shifts to higher values as the monolayer is compressed. A Bragg peak at this momentum transfer, is commonly observed in Langmuir monolayers of long-chain amphiphiles (Kaganer et al., 1999) corresponding to the hexagonal crystallization of individual hydrocarbon chains with a lattice constant $a \approx 4.81$ Å, and a cross-section $\approx$ 20.0 Å^2 per alkyl chain (or 40.0 Å^2 per molecule).

At large molecular areas ($\pi \approx 0.6$ mN/m; $A \approx 58$ Å^2), in addition to the central peak ($Q_{xy} \approx 1.5$ Å^{-1}) due to the hexagonal structure, two Bragg reflections, with a surface pressure dependence that is different from that of the central peak, are observed at $Q_{xy} \approx 1.43$ Å^{-1}, and $Q_{xy} \approx 1.60$ Å^{-1} (Fig. 4). As the monolayer is compressed, the intensity of these peaks changes only slightly, and they are observed even at the highest pressures, as shown in Fig. 5. Whereas the linewidth of the reflection associated with the hexagonal symmetry is relatively broad at large molecular areas, the two satellites are almost resolution-limited. This is evidence for the presence of two length scales in the crystalline domains, one associated with the hexagonal phase and the other with a second crystalline phase. We propose that the extra Bragg reflections are due to the formation of a secondary, 2D orthorhombic structure, with lattice constants $a_{orth} \approx 5.30$ Å, $b_{orth} \approx 7.84$ Å ($\pi \approx 0$) which correspond to a cross-section of $\approx$20.80 Å^2 per chain. Table II lists the in-plane structural parameters at various molecular areas. Similar Bragg reflections were also seen in the X-ray diffraction pattern of bulk ceramides, in particular when mixed with $\approx$10% cholesterol (Bouwstra et al., 1996).

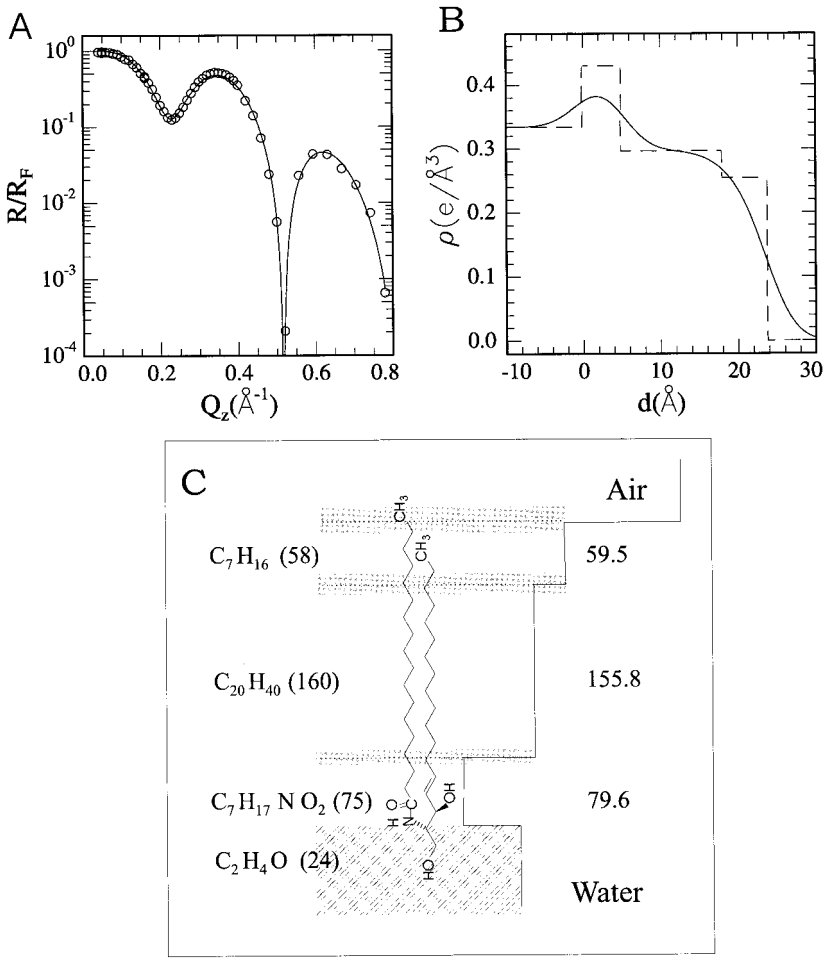

FIGURE 3 Normalized reflectivity from a ceramide monolayer at $\pi = 36$ mN/m measured at the NSLS (*A*). The dashed line is the best fit to the data using a three-slab model with a corresponding electron density profile shown as a dashed line in *B*. A possible division of the molecule within the three slab model is shown in *C*. The molecular sections and the number of electrons per section (in parentheses) were compared with the numbers derived from the electron density profile (*right side of the figure*), using Eq. 9.

The intensity along the Bragg rod (see Fig. 4) is analyzed in the framework of the distorted wave BA (DWBA) using (Vineyard, 1982)

$$I \propto |t(k_{z,i})|^2 |F(Q_z)|^2 e^{-(Q_z\sigma_{eff})^2} |t(k_{z,f})|^2 \qquad (5)$$

where $t(k_{z,f}) = 2k_{z,f}/(k_{z,f} + \sqrt{k_{z,f}^2 - k_c^2})$, and a similar expression for $t(k_{z,i})$, is the Fresnel transmission function, which gives rise to an enhancement around $k_c = k_0 \sin \alpha_c$, as seen in Fig. 4. The structure factor for the alkyl chain with length d is given to a good approximation (Kjaer et al., 1989) by

$$F(Q_\zeta) = \frac{\sin(Q_\zeta d/2)}{Q_\zeta d/2}, \qquad (6)$$

where ζ is parallel to the chain of the molecule. The chains are tilted with respect to the surface normal at an angle, t, in an azimuthal tilt direction, ϕ_0. In the present study, the tilt direction is measured from the $(1\bar{1})$ reflection, where $\phi_0 = 0$ corresponds to a tilt toward next nearest neighbors (NNN) and $\phi_0 = 30°$ is a tilt toward nearest neighbors (NN). In the case of a uniform tilt, the chain structure factor, Eq. 6, is modified for each reflection i by transforming Q_ζ as follows

$$Q_\zeta = -\sin t(Q_x \cos\phi_i - Q_y \sin\phi_i) + Q_z \cos t \qquad (7)$$

where ϕ_i is measured from the $(1\bar{1})$ and includes the angle of the tilt direction ϕ_0. If the alkyl chains are uniformly tilted with respect to the surface normal, the six degenerate fundamental Bragg reflections of the hexagonal phase give rise to inequivalent Bragg reflections with different rod profiles. In addition, the tilt can introduce new symmetries that split the primary Bragg reflection into two (orthorhombic) or three (oblique) distinct reflections. Because of the 2D-like polycrystalline (mosaic) character of the monolayer, all relevant orientations must be considered in the analysis of a rod scan. The fit to the rod scan in Fig. 5 using Eqs. 5–7 yields a range of values to the variable parameters, with $d = 17 \pm 6$ Å, $t = 0 \pm 4°$, and $\sigma = 3.7 \pm 1$ Å. The solid line in Fig. 4 is the best fit to the data using $d = 13$ Å, $t = 0$ degrees, and $\sigma = 4.3$ Å, which is consistent with the ordering of the intermediate hydrocarbon layer inferred from the reflectivity data.

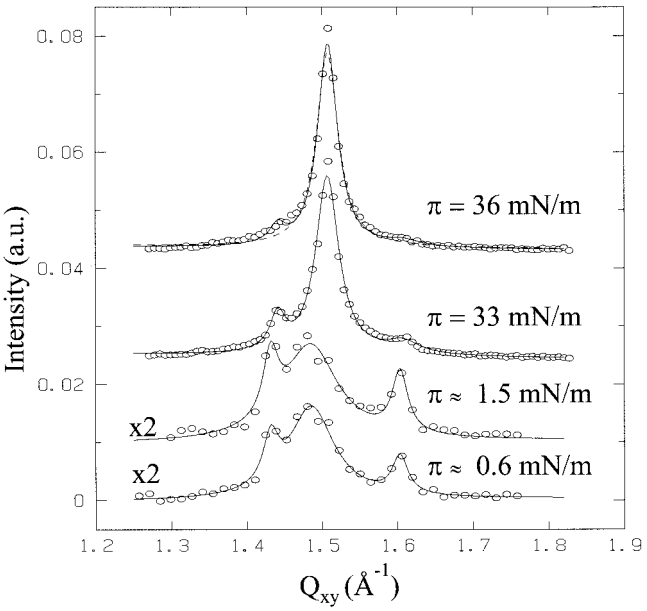

FIGURE 4 Diffraction patterns from a C18-ceramide monolayer at the air-water interface at various surface pressures.

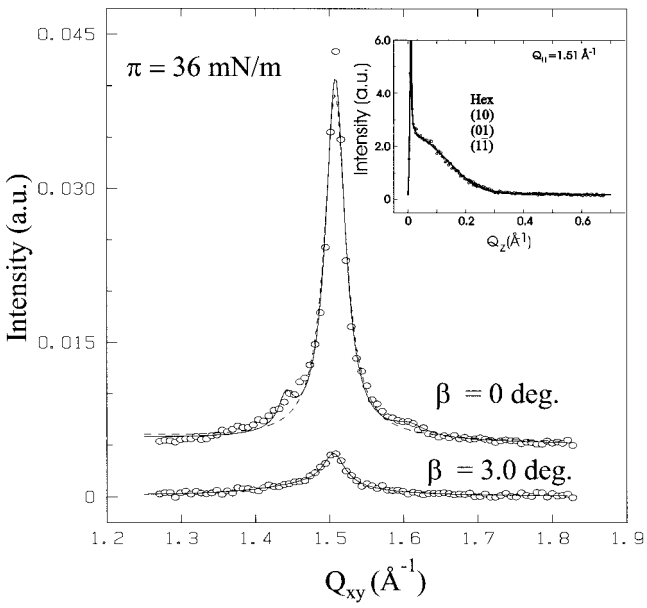

FIGURE 5 Diffraction pattern from a C18-ceramide monolayer at the air-water interface taken at $\pi = 33$ mN/m at the horizon ($\beta = 0$) and across the rod at $\beta = 3°$. The fit to a single Lorentzian is shown with a dashed line, whereas the solid line includes extra peaks at positions that are observed at lower pressures.

DISCUSSION

In-plane ordering and phase-separation

In general the packing of hydrocarbon chains (alkanes, lipids, fatty acids, etc.) is in the form of a slightly distorted hexagonal lattice as observed at high pressures in this study. In the hexagonal (rotator) phase, the all-trans hydrocarbon chains rotate partially around their long axes, which effectively gives a cylindrical shape to each chain (Small, 1986). Due to inter-chain interactions, which depend on pressure and temperature, the rotational degrees of freedom are suppressed and the chains assume lower 2D symmetries, such as orthorhombic or oblique (Small, 1986). Fundamental Bragg reflections in the orthorhombic phase with indices (11), (1$\bar{1}$), and (02) are then equivalent to the original hexagonal reflections (10), (01), and (1$\bar{1}$), respectively (but distorted). We argue that a change in symmetry from hexagonal to orthorhombic or oblique can also be driven by strong interactions in the headgroup region, which may lead, due to steric hindrances, to structures that are incompatible with conventional packing of alkyl chains. This is especially important in the case of sphingolipids, where headgroups are likely to form strong hydrogen bonds between hydroxyl and amide groups.

The predominant GID peak and the rod scan at high pressures (Fig. 5) are clear signatures of a relatively simple hexagonal arrangement of hydrocarbon chains with practically zero tilt angle with respect to the surface-normal ($\leq 4°$). A similar hexagonal structure was observed in a recent study of the two-chain lipid dihexadecyl phosphate (DHDP) in Langmuir monolayers (Gregory et al., 1999). However, the DHDP monolayer exhibits a single peak at all surface pressures, with no indication of extra Bragg reflections as seen in the present study. In the case of DHDP, the phosphate headgroups are negatively charged, which by symmetry reinforces a simple hexagonal packing. Ceramide monolayers, on the other hand, comprise hexagonal and orthorhombic phases in coexistence (Fig. 4). Both of these phases incorporate densely packed hydrocarbon chains with molecular areas $A_0 \approx 41.5$ Å^2, although the average molecular area as obtained from the isotherm is significantly larger, $A_{iso} \approx 57.5$ Å^2. The large discrepancy between A_{iso} and A_0 implies surface coverage of 75% crystalline domains, with domains that are most likely surrounded by pure water and/or low density uncorrelated lipids (2D lipid gas phase). Domain formation of crystalline phase surrounded by a 2D lipid liquid was reported for monolayers of the phospholipid dimyristoyl phosphatidic acid (DMPA) (Helm et al., 1987) with a diffraction pattern that consisted of a single Bragg peak that varied in position and width upon compression of the monolayer. In that case, the Bragg peak appeared only at elevated pressures ($\pi \approx 15$ mN/m ≈ 50 Å^2), above the phase transition onset pressure $\pi_c \approx 8$ mN/m. Ceramide, on the other hand, exhibits a diffraction pattern with several uncorrelated Bragg reflections that appear at a range of molecular areas where the surface pressure is practically zero, suggestive of crystalline domains in a 2D lipid-gas environment. The peaks associated with the orthorhombic phase vary just slightly with the compression of the film. We argue that the formation of the orthorhombic

phase is driven by strong hydrogen bonding among ceramide headgroups in an arrangement that is incompatible with the common hexagonal packing of the alkyl chains. Although the peaks associated with the orthorhombic structure appear weak compared to the main hexagonal peak at high pressures, our analysis shows that their intensities vary just slightly as the monolayer is compressed. That indicates that the number of these domains and their sizes are practically constant throughout the isotherm. In particular, this implies that at high pressures, when the monolayer is intact, these orthorhombic domains are distributed in a predominantly hexagonal environment. Since it is unlikely that a system consisting of one type of molecules will condense into two types of structures on an isotropic substrate (water surface), we suggest that initially the orthorhombic crystals are formed and they subsequently act as nucleation centers around which hexagonal structure evolves. Thus, the two symmetries coexist in the same domains and at high pressures (high density) the attractive van der Waals interactions among chains become dominant, leading to the growth of the hexagonal phase, surrounding the orthorhombic domains. However, the interactions among the hydrocarbon tails are not sufficiently strong to bring about the herringbone order (Kaganer et al., 1999) at any pressure of the monolayer.

The reflectivity experiments also support the phase separation into crystalline domains that coexist with 2D gas phase lipid at large molecular areas. The reflectivity curve at $A = 69$ Å^2 per molecule (Fig. 2) resembles those at much smaller areas in the crystalline phase, showing that at relatively large molecular areas there is a high degree of organization in the film. However, at this area the simple two-slab model did not yield a reasonable fit to the reflectivity curve. Therefore, based on the phase separation model discussed above, and without introducing any extra parameters, we analyzed the reflectivity curve assuming incoherent scattering from two domains as follows

$$R(Q_z) = pR_{cer}(Q_z) + (1 - p)R_{H_2O}(Q_z) \qquad (8)$$

where $p = A_0/A_{iso} \approx 0.6$ equals the partial coverage of the surface with nearly densely packed aggregates and R_{H_2O} is the reflectivity of pure water. At very large molecular areas ($A = 101$ Å^2; see Fig. 2) the reflectivity is practically that of pure water surface, R_{H_2O}, which is therefore reasonable to be used in Eq. 8.

Aggregation of ceramide molecules at relatively large molecular areas was in fact inferred from systematic examination of the $\pi - A$ isotherm, as mentioned above (Löfgren and Pascher, 1977). Based on the reflectivity measurements, and the derivative of surface pressure with respect to the molecular area (Fig. 1), we suggest that for pressures $\pi \geq 3$ mN/m ($A_{iso} \approx 45$ Å^2), the aggregates coalesce into an infinite domain, giving rise to the abrupt increase of surface pressure versus molecular area. This coalescence and the macroscopic characteristics of the phase-separation in ceramide monolayers might be further examined by fluorescence microscopy (Lösche et al., 1983) and/or Brewster angle microscopy (Henon and Muenier, 1991; Hönig and Möbius, 1991), which are not available to us at this time.

Molecular interpretation of the electron density across the interface

The correspondence between the slab-model of the electron density and the structure is almost straightforward for many amphiphiles (Vaknin et al., 1991; Schalke et al., 2000). Using the reflectivity results in conjunction with the GID, a molecular level interpretation of the electron density across the interface can be obtained. Since the area per molecule, A_m, is known, the total number of electrons per molecule, N_{total}, can be determined as

$$N_{total} = A_m \int \rho(z)dz = A_m \sum_j \rho_j d_j \qquad (9)$$

where at elevated pressures the molecular area A_m can be obtained from the isotherm ($A_m \equiv A_{iso}$) or from the diffraction pattern ($A_m \equiv A_0$). Using the isotherm, has the disadvantage of having relatively large uncertainties that cannot be estimated, such as adsorption of molecules to the trough's boundaries, formation of soluble clusters, or the inclusion of surfactant impurities. On the other hand, using the diffraction-extracted molecular area has the advantage of being more accurate, although it ignores all contributions to the reflectivity from point defects, domain boundaries, and phase-separated regions.

Here, we discuss the molecular structure at 36 mN/m where the diffraction yields 40 ± 0.1 Å^2 (the isotherm gives 39 ± 1.0 Å^2; analysis of reflectivities taken at 27 and 33 mN/m yield similar results). Using the GID-extracted molecular area (40.06 Å^2), Eq. 9 yields $N_{total} = 294.9 \pm 4$ electrons per molecule. The total number of electrons in one ceramide molecule is, $N_{total}^{cer} = 317$. To explain the difference, we suggest that the missing electrons are those at the tip of the headgroup region, including the CH-CH$_2$-OH group. This portion of the molecule is surrounded by water molecules ($\approx$2 H_2O molecules per ceramide), forming a slab that has essentially the same electron density as water and is therefore practically not detected in the X-ray reflectivity measurements. The number of electrons in the molecule without the CH-CH$_2$-OH group is 293, which is in reasonable agreement with the number extracted from the reflectivity (294.9 electrons). With an estimated length of 3.3 Å and a molecular area $A_m \approx 40$ Å^2, the CH-CH$_2$-OH group with two water molecules gives electron density that is the same as that of water (0.334 e/Å^3). Furthermore, this model is supported by the examination of the total length of the molecule and its tilt from the surface normal. The length

TABLE 1 Three-slab model parameters used to fit the reflectivity data in Fig. 3 for C18-ceramide monolayer on H_2O

	Values	
Independent variables		
d_{head} (Å)	$4.65 \pm {}^{1.0}_{0.6}$	headgroup layer thickness
ρ_{head} (e/Å^3)	$0.43 \pm {}^{0.3}_{0.15}$	electron density of headgroup
$d_{tail,1}$ (Å)	$13.12 \pm {}^{0.4}_{0.4}$	thickness of intermediate tail slab
$\rho_{tail,1}$ (e/Å^3)	$0.297 \pm {}^{0.015}_{0.005}$	electron density of intermediate tail slab
$d_{tail,2}$ (Å)	$5.9 \pm {}^{1.2}_{0.9}$	thickness of upper tail slab
$\rho_{tail,2}$ (e/Å^3)	$0.256 \pm {}^{0.010}_{0.010}$	electron density of upper tail slab
σ (Å)	$2.99 \pm {}^{0.15}_{0.10}$	interfacial roughness
Dependent variables		
d_{total} (Å)	$23.6 \pm {}^{0.8}_{0.5}$	total thickness of interfacial layer
N_{total}/A_m (e/Å^2)	$7.4 \pm {}^{0.1}_{0.2}$	2D surface layer electron density

of the molecule estimated from a molecular model $d_{total}^{model} = 26.5 \pm 0.5$ Å, is larger than the value extracted from the reflectivity $d_{total}^{exp} = 23.6 \pm 0.8$ Å, and the difference can be attributed to the "missing" CH-CH_2-OH group. The difference between the two lengths cannot be explained by a tilt of the alkyl chains from the surface-normal, since this would imply a tilt angle of about 30°, which is not consistent with the rod scans or reflected in the total length associated with the chains in the electron density model, as discussed below. One important consequence of this interpretation of the electron density profile is that water penetration into the film is confined to the tip of the molecule so that any other part of the molecule is essentially dehydrated.

To associate the different slabs with different parts of the molecule we proceed by calculating the number of electrons in the tail as

$$N_{e,tail} = \rho_{tail}(A_m d_{tail}) . \quad (10)$$

and a similar expression for the headgroup. As shown in Table 1, a possible division of the molecule into the different slabs is depicted in Fig. 3 *C*. There are two features in this division that are unusual compared to other lipids. One is that two slabs are required to describe the alkyl chains of which one, with lower density, is at the air interface, and the other is that the major part of the headgroup is essentially dehydrated. These two features were qualitatively found in any model we tested. A possible explanation for the division of the alkyl chain region into two slabs is the difference in the length between the two chains emanating from the headgroup of C18 ceramide. However, that does not explain the location of the interface between the headgroup and the chains. Based on recent X-ray reflectivities of sphingosine and other sphingolipids that exhibit similar characteristics, we propose that these features result from NN staggering along the surface-normal (Vaknin and Kelley, unpublished results). Due to hydrogen bonding between the amide carbonyl of one molecule and the hydroxyl group of another, two neighboring molecules can bind at different positions with respect to the water interface. Such inhomogeneity on the molecular length scale can create staggered chains at the air interface, that would effectively make the top most layer less dense. Consequently, the depiction of the molecule in Fig. 3 *C* is too simplistic; a more realistic model should include more than one molecule.

Since the electron density associated with the intermediate-chain region is close to that of crystalline alkyl chains, the tilt angle of the chain with respect to the surface normal *t* can be estimated from the reflectivity by (Kjaer et al., 1989).

$$d_{tail}/l_{tail} = \cos t \quad (11)$$

where l_{tail} is the length of the fully extended tail. The methylene spacing projected onto the chain axis for crystalline saturated alkyl tails $d_{C-C} = 1.265 \pm 0.010$ Å, and for a terminal CH_3 group is $9/8 d_{C-C}$ (Kjaer et al., 1989). It follows that the length of the intermediate layer with carbon chains, $d_{tail,1} = 13$ Å is in reasonable agreement with that expected from 10 C—C bonds (~12.7 Å), which suggests that this portion is practically untilted. The rod scan analysis discussed above suggests $t = 0 \pm 4°$.

CONCLUSIONS

Using X-ray reflectivity and diffraction at grazing angles of incidence (GID) we have encountered unique features that

TABLE 2 Structural parameters extracted from the GID data shown in Fig. 4. The proposed model consists of two types of 2D crystals (hexagonal and orthorhombic). The inplane *d*-spacing and the lattice constant *a* for the hexagonal structure are also listed below.

		Orthorhombic domains				
A_{iso} (Å^2)	π (mN/m)	$Q_{(11)+(1\bar{1})}$ (Å^{-1})	$Q_{(02)}$ (Å^{-1})	a_{orth} (Å)	b_{orth} (Å)	A_{calc} (Å^2)
57	0.6	1.432	1.603	5.295	7.84	41.5
52	1.5	1.432	1.603	5.295	7.84	41.5
39.0	33.0	1.440	1.607	5.258	7.82	41.12
		Hexagonal domains				
A_{iso} (Å^2)	π (mN/m)	Q_{hex} (Å^{-1})	d (Å)	a (Å)		A_{calc} (Å^2)
57–52	0.6 –1.5	1.48	4.245	4.90		41.6
38–40	33 –36	1.508	4.167	4.811		40.09

are specific to the organization of C18-ceramide in a monomolecular film at the air water interface. In addition to the frequently observed hexagonal packing of the hydrocarbon chains we find an orthorhombic phase that coexists with the hexagonal symmetry. The 2D crystals are formed at relatively large molecular areas indicating a phase separation between ordered domains and 2D lipid gas phase. It is argued that aggregation to orthorhombic crystals may be induced by the relatively strong hydrogen bonding between neighboring molecules, such that the headgroups are packed in an arrangement that is incompatible with the conventional hexagonal chain packing. While the orthorhombic structure is incommensurate (Durbin et al., 1998) with the simple hexagonal arrangement, the orthorhombic crystals apparently act as nucleation centers for the formation of the conventional hexagonal phase at very low pressures. As the density in the monolayer increases upon compression, attractive van der Waals interactions among chains become dominant and lead to a predominantly hexagonal chain ordering. However, these interactions are not strong enough to bring about the more closely packed herringbone-like orthorhombic structures observed in different lipid monolayers (Kaganer et al., 1999). The X-ray reflectivities of the monolayers strongly suggest that the arrangement of the molecules in the film is such that NN sites are not equivalent, which was not observed before with lipid monolayers.

We thank B. M. Ocko for helping with the experiments and for helpful advice, and M. Lösche for many helpful suggestions. Ames Laboratory is operated for the U.S. Department of Energy by Iowa State University under contract no. W-7405-Eng-82. The work at Ames was supported by the Director for Energy Research, Office of Basic Energy Sciences.

REFERENCES

Abrahamsson, S., B. Dahlén, H. Löfgren, I. Pascher, and S. Sundell. 1976. Molecular arrangement and conformation of lipids of relevance to membrane structure. *In Structure of Biological Membranes. Edited by S. Abrahamsson and I. Pascher. Plenum Press, New York.* 1–21.

Als-Nielsen, J. and Kjaer, K. 1989. Phase transitions in soft condensed matter. *Proc. NATO ASI Ser. B.* 211:113.

Bouwstra, J. A., G. S. Gooris, K. Cheng, K. A., Weerheim, W. Bras, and M. Ponec. 1996. Phase behavior of isolated skin lipids. *J. Lipid Res.* 37:999–1011.

Durbin, M. K., A. G. Richter, C.-J. Yu, J. Kmetko, and P. Dutta. 1998. Backbone orientational order in fatty acid monolayers at the air-water interface. *Phys. Rev. E.* 58:7686–7690.

Garson, J., J. Doucet, J. Lévêque, and G. Tsouceris. 1991. Oriented structure in human stratum corneum revealed by x-ray diffraction. *J. Invest. Dermatol.* 96:43–49.

Gray, G. M., and H. J. Yardley. 1975. Different populations of pig epidermal cells: isolation and lipid composition. *J. Lipid Res.* 16: 441–447.

Gregory, B. W., D. Vaknin, J. D. Gray, B. M. Ocko, T. M. Cotton, and W. S. Struve. 1999. Two dimensional crystallization of phthalocyanine pigments at the air/water interface. *Phys. Chem. B.* 103:502–508.

Hannun, Y. A. 1994. The sphingomyelin cycle and the second messenger function of ceramide. *J. Biol. Chem.* 269:3125–3128.

Hauser, J. M., B. M. Buehrer, and R. M. Bell. 1994. Role of ceramide in mitogenesis induced by exogenous sphingoid bases. *J. Biol. Chem.* 269:6803–6809.

Helm, C. A., H. Möhwald, K. Kjaer, and J. Als-Nielsen. 1987. Phospholipid monolayers between fluid and solid states. *Biophys. J.* 52:381–390.

Henon, S., and J. Muenier. 1991. Microscopic at the Brewster angle: Direct observation of phase-order phase transitions in monolayers. *Rev. Sci. Instrum.* 62:936–939.

Hönig, D., and D. Möbius. 1991. Direct visualization of monolayers at the air-water interface by Brewster angle microscopy. *J. Phys. Chem.* 95: 34590–34592.

Kaganer, V. M., H. Möhwald, and P. Dutta. 1999. Structure and phase transitions in Langmuir monolayers. *Rev. Mod. Phys.* 71:779–819.

Kjaer, K., J. Als-Nielsen, C. A. Helm, P. Tippman-Krayer, and H. Möhwald. 1989. Synchrotron x-ray diffraction and reflection studies of arachidic acid monolayers at the air-water interface. *J. Phys. Chem.* 93:3200–3206.

Löfgren, H., and I. Pascher. 1977. Molecular arrangements of sphingolipids. The monolayer behavior of ceramides. *Chem. Phys. Lipids.* 20: 273–284.

Lösche, M., E. Sackmann, and H. Möhwald. 1983. A fluorescence microscopic study concerning the phase diagram of phospholipids. *Ber. Bunsenges. Phys. Chem.* 87:848–852.

Ocko, B. M., X. Z. Wu, E. B. Sirota, S. K. Sinha, O. Gang, and M. Deautch. 1997. Surface freezing in chain molecules: Normal alkanes. *Phys. Rev. E.* 55:3164–3182.

Parratt, L. G. 1954. Surface studies of solids by total reflection of x-rays. *Phys. Rev.* 59:359–369.

Schalke, M., P. Krüger, M. Weygand, and M. Lösche. 2000. Submolecular organization of DMPA in surface monolayers: beyond the two-layer model. *Biochim. Biophys. Acta.* 1464:113–126.

Schwartz, D. K., M. L. Schlossman, and P. S. Pershan. 1992. Reentrant appearance of the phases in a relaxed Langmuir monolayer of the tetracosanoic acid as determined by x-ray scattering. *J. Chem. Phys.* 96:2356–2370.

Shah, D., J. M. Atienza, R. I. Duclos, A. V. Rawlings, Z. Dong, and G. G. Shipley. 1995. Structure and thermotropic properties of synthetic c16:0 (palmitoyl) ceramide: effect of hydration. *J. Lipid Res.* 36:1936–1944.

Small, D. M. 1986. *The Physical Chemistry of Lipids.* Plenum Press, New York.

Spiegel, S., and A. H. Merrill. 1996. Sphingolipid metabolism and cell growth regulation. *FASEB J.* 10:1388–1397.

Vaknin, D., K. Kjaer, J. Als-Nielsen, and M. Lösche. 1991. Structural properties of phosphotidylcholine at the air/water interface: neutron reflection study and reexamination of x-ray reflection experiments. *Biophys. J.* 59:1325–1332.

Vineyard, G. 1982. Grazing-incidence diffraction and distorted wave approximation for the study of surface. *Phys. Rev. B.* 26:4146–4159.